Resolution of the Ba $(6p_jnd_j)_1$ and $(6p_jnd_j)_3$ autoionizing states and their mixing with the $(6p_jns_{1/2})_1$ and $(6p_jng_j)_3$ states

R. Kachru, H. B. van Linden van den Heuvell, and T. F. Gallagher
Molecular Physics Department, SRI International, Menlo Park, California 94025
(Received 23 July 1984)

We report the resolution of the Ba $(6p_jnd_j)_{J=1}$ and $(6p_jnd_j)_{J=3}$ autoionizing levels and their mixing with the $(6p_jns_{1/2})_{J=1}$ and $(6p_jng_j)_{J=3}$ states by a three-step laser excitation approach. For the $6p_{1/2}nd_j$ levels we are unable to discern a difference between $J=1$ and $J=3$. For the $6p_{3/2}nd$ levels we are able to identify the two $J=3$ states, but only one $J=1$ feature, and measure their quantum defects. Furthermore we are able to measure the mixing of the $(6p_{3/2}nd_j)_{J=1}$ states with the $(6p_{3/2}ns_{1/2})_{J=1}$ states and determine that the analogous mixing of the $(6p_{3/2}nd_j)_{J=3}$ states with the $(6p_{3/2}ng_j)_{J=3}$ states is not observable, nor is any mixing of the $6p_{1/2}nd_j$ states with either $6p_{1/2}ns_{1/2}$ or $6p_{1/2}ng_j$ states.

I. INTRODUCTION

In doubly excited atomic states, such as the Ba $6p_jnd_j$ states there are typically several values of the total angular momentum J, which reflect the relative orientations of the angular momenta of the two excited electrons, the $6p_j$ and nd_j electrons in the example above. Although the value of J is expected to affect both the energy and autoionization rate of a doubly excited state, to date there has been little systematic investigation of the J dependence of these parameters. In many previous experiments only one value of J or an ill-defined mixture has been studied. For example, in vuv single-photon excitation from the Ba $J=0$ ground state only $J=1$ states may be excited. On the other hand, in an experiment involving collisional excitation several J values are usually allowed. In principle a multistep laser excitation scheme allows the population of several J states in a well-defined manner, and this approach has previously been used to determine the energy levels and autoionization rates of the Ba $6p_j20s_{1/2}$ states.[1] A particularly notable result of this work is the fact that the autoionization width of $(6p_{3/2}ns_{1/2})_{J=1}$ state is 12 cm^{-1} while the widths of all other $(6p_jns_{1/2})_J$ states are 3 cm^{-1}.[1]

Here, we report the study of the $6p_jnd_j$, $J=1$ and $J=3$ states as a systematic comparison of the effects of the relative orientation of the angular momenta of the two electrons. Our choice of the $J=1$ and 3 states is based on experimental considerations relevant to our three-step photoexcitation method. With all three exciting lasers circularly polarized in the same sense we observe a pure $J=3$ spectrum. With all three lasers linearly polarized in the same direction, we observe a spectrum consisting of only $J=1$ and $J=3$ states from which the $J=3$ states may be subtracted to obtain the $J=1$ spectrum. Since the states under study are autoionizing, we observe broad line shapes not discrete lines, so it is not realistic to expect to unravel more than two series of states. Thus, we have not studied the $J=0$ and 2 states.

In addition we have employed a rather novel technique to investigate the mixing of different $6pnl$ states of the same parity and J. The technique is based on using the high power of the exciting laser to bring out very small spectral features indicative of such mixing. In this paper we describe briefly the experimental approach, the results obtained, and the conclusions drawn from them.

II. EXPERIMENTAL APPROACH

The method used in these experiments is indicated schematically in the energy-level diagram of Fig. 1 in which the relevant levels for the study of the autoionizing $6p_{3/2}15d_j$ levels are shown. As shown by the arrows of Fig. 1, we use three laser pumping steps to reach an autoionizing $6pnd$ state which promptly decays into an ion and an electron either of which we may detect.

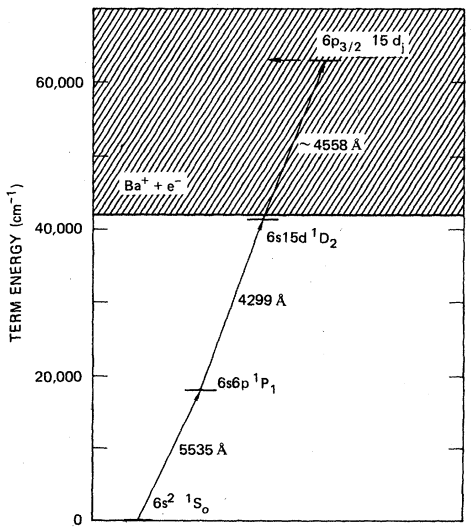

FIG. 1. Energy levels for the study of the autoionizing Ba $6p_{3/2}15d_j$ levels. The three laser pumping steps are shown by the nearly vertical arrows, and the decay of the autoionizing state to an ion and an electron is shown by the horizontal arrow.

The apparatus has been described elsewhere so our description here is brief.[2] A frequency doubled and tripled Nd:YAG (yttrium aluminum garnet) laser is used to pump three dye lasers for the three pumping steps shown in Fig. 1. The 5-ns dye laser pulses are sequential in time and have pulse energies of 100 μJ and linewidths of 1 cm^{-1}. An effusive atomic beam of Ba passes between a plate and a grid where it is intersected at a right angle by the three spatially overlapping dye laser beams. An atom excited to an autoionizing state promptly decays into an ion and an electron. Approximately 200 ns after the laser pulses we apply a positive voltage pulse to the plate pushing any ions formed through the grid to a venetian blind electron multiplier. Thus the ion signal is proportional to the number of atoms excited to the autoionizing state.

The optical spectra, whether obtained with high or low third laser power, are recorded by setting the wavelengths of the first two lasers to excite a bound $6snd$ Rydberg state, the energy of which is known,[3] and observing the ion signal as the wavelength of the third laser is scanned. In a low power spectrum we typically observe one transition, to the $6pnd$ state, which is very near one of the Ba^+ resonance lines at 4555 or 4935 Å. This is essentially the Ba^+ $6s$-$6p$ transition with the outer nd electron a spectator.[4] The transition is broadened by the autoionization of the $6pnd$ state, and the ion signal recorded is, to an excellent approximation, a faithful reproduction of the profile of the autoionizing state, thus we may readily determine the position and width of the autoionizing $6pnd$ state. The direct excitation to the underlying continua is so small that there is no measurable interference. In the high power spectra, the central feature corresponding to the $6snd \rightarrow 6pnd$ transition is completely saturated,[5] but many small satellite features emerge in the wings of the line which correspond to the outer electron changing its principal quantum number as the inner electron makes the $6s$-$6p$ transition.[32]

The relative frequency scale for the third laser scans is obtained by simultaneously monitoring the transmission of the third laser through a 3.52 cm^{-1} free-spectral-range etalon. The absolute value of the scale is fixed by observing the coincidence at which the third laser drives both the transition from the $6s\,6p\ ^1P_1$ state to a known bound state[3] and the transition to an autoionizing state. In Table I we list these transitions which serve as frequency markers.

TABLE I. Two-photon coincidence lines.[a]

Transition	$h\nu$ (cm^{-1})
$6s6p\ ^1P_1 \rightarrow 6s11d\ ^1D_2$	22423.3
$6s12s\ ^1S_0$	22173.5
$5d8s\ ^1D_2$	22163.5
$6s10d\ ^1D_2$	21938.1
$6s10d\ ^3D_2$	21861.9
$6s11s\ ^1S_0$	21611.6
$5d8s\ ^3D_2$	21404.7

[a]See Ref. 3.

III. RESOLUTION OF THE $(6p_{3/2}nd_j)_{J=1}$ AND $(6p_{3/2}nd_j)_{J=3}$ STATES

The most straightforward approach to resolving the $(6p_{3/2}nd_j)_{J=1}$ and $(6p_{3/2}nd_j)_{J=3}$ states is through selective excitation of these states by polarizing the excitation laser pulses. If all lasers used in our laser excitation scheme are circularly polarized it is evident that only $J=3$ excited states can be produced. On the other hand, by linearly polarizing the lasers both $J=3$ and $J=1$ states can be excited. Thus, those excitation features observed with linearly polarized light but not with circularly polarized light are due to the $J=1$ states. Once the $J=3$ states are identified, the remaining features are $J=1$. Typical excitation spectra of the $6p_{3/2}nd$ states are shown in Fig. 2. In obtaining these spectra, the first and second laser frequencies are fixed, with the first and the second lasers tuned to the $6s^2\ ^1S_0$–$6s6p\ ^1P_1$ and $6s6p\ ^1P_1$–$6snd\ ^1D_2$ transitions, respectively. In Fig. 2(a) all lasers are circularly polarized to excite only $J=3$, and in Fig. 2(b) all lasers are linearly polarized to excite both $J=1$ and $J=3$. The third dye laser frequency is scanned near the Ba^+ $6s_{1/2}$-$6p_{3/2}$ transition, where it excites the bound $6snd\ ^1D_2$ Ba atoms to the $(6p_{3/2}nd_j)_{J=1,3}$ states which subsequently autoionize. Scanning the third laser frequency and collecting the ions formed as a result of the decay of the autoionizing states results in an excitation spectrum shown in Fig. 2. In obtaining such spectra, the intensity of the third dye laser intensity is reduced by neutral density filters until the observed ion signal varies linearly as a function of the laser intensity. Thus the observed signal is proportional to the photoexcitation cross section. As noted earlier a higher third laser intensity in these measurements results in a saturation effect which has been termed depletion broadening[5] and will be discussed later. Figure 2(a) shows the spectrum obtained with all lasers circularly polarized and the trace obtained with the lasers linearly polarized is shown in Fig. 2(b). The three distinct features seen in Fig. 2(b) are labeled I, II, and III, respectively. Features I and II are observed with the circularly polarized light as shown in Fig. 2(a) whereas the last feature is only observed with linearly polarized light. This leads us to conclude that features I and II are the excitation spectrum of $J=3$ states. The remaining feature corresponds to an excitation of a $J=1$ state. Note that the last feature is manifested as an asymmetric tail on the high-frequency side of the central peak. We can determine the position and the width of the $J=1$ state by assuming that the observed composite line shape on the higher frequency end of feature I is due to a partial overlap of two Lorentzian lines, one being $J=3$ and the other $J=1$. Similar measurements were performed on several states with $13 \leq n \leq 20$. The quantum defects and widths of these states are tabulated in Table II.

There are several important features that emerge from our measurements. First, we are able to observe three distinct states pertaining to the $6p_{3/2}nd_{5/2\,(3/2)}$ series that converge to the $6p_{3/2}$ limit of Ba^+. We note that Gounand *et al.*[6] in their previous study of $(6p_{3/2}nd_j)_{J=3}$ series measured the position and widths of the central

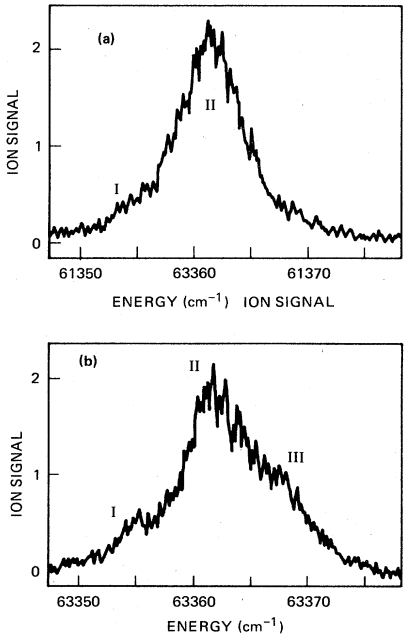

FIG. 2. Ion signals recorded as the third laser frequency is scanned with the first two lasers set to populate $6s17d\ ^1D_2$ Rydberg state with all three lasers (a) circularly polarized and (b) linearly polarized. The prominent features in this experimental trace are labeled I, II, and III (see text).

$J=3$ feature for n ranging from 10 to 22. As our present experiments indicate, there are in fact two $J=3$ states, although the oscillator strength for exciting these states from the bound $6snd\ ^1D_2$ Rydberg states are in ratio 1:15 for these two states. The second interesting aspect of our measurement is that we do not observe two distinct $J=1$ states, although there should be two $J=1$ states belonging to the $(6p_{3/2}nd_j)_{J=1}$ series. Either we are unable to resolve the pair of $J=1$ states or else the two $J=1$ states are degenerate with each other or one of the $J=3$ states.

Since the central $J=3$ feature observed in our measurements is much larger than the other features, and in particular the second $J=3$ feature, we are unable to accurately measure the widths of these states. This is primarily due to the considerations of signal to noise in our experiment. For instance if we try to increase the amplitude of the small $J=3$ feature by increasing the intensity of their third laser, we also increase the width of the central feature due to depletion broadening. The depletion broadening leads to the masking of smaller features due to the growing amplitude of the wings of the central $J=3$ line profile.

TABLE II. Quantum defects (relative to the Ba^+ $6p_{3/2}$ limit) of the three subfeatures observed in the Ba $(6p_{3/2}nd_j)_{J=1,3}$ excitation spectrum.

State	Quantum defect of feature I	II	III
$6p_{3/2}13d_j$	2.897(5)	2.750(5)	2.627(5)
$6p_{3/2}15d_j$	2.894(5)	2.739(5)	2.629(5)
$6p_{3/2}16d_j$	2.883(5)	2.738(5)	2.618(5)
$6p_{3/2}17d_j$	2.890(5)	2.753(5)	2.603(5)
$6p_{3/2}20d_j$	2.878(5)	2.742(5)	2.608(5)

IV. DISCUSSION

The separation Δ_{21} between features II and I, which corresponds to the energy splitting of the two $J=3$ states, is plotted as a function of $(n^*)^3$, where n^* is the effective quantum number, on a log-log scale in Fig. 3. A similar plot of Δ_{32} which corresponds to the splitting between the higher-lying $J=3$ state and the $J=1$ state is shown in Fig. 4. The solid lines in Figs. 3 and 4 have a slope of -1. It is not entirely surprising that these splittings scale as $(n^*)^{-3}$, since both the electrostatic and the spin-orbit splittings scale as $(n^*)^{-3}$. Since the spin-orbit coupling of the core electron is much greater than either the spin-orbit coupling of the outer electron or the electrostatic coupling of the electrons, we can adopt the intermediate, or *Kl*, coupling scheme to estimate the observed splittings. If we assume that the observed splittings of the two-electron state are entirely due to the spin-orbit coupling of the Rydberg electron, then the two $J=3$ states should lie between the two $J=1$ states. Our experiment indicates that at least one $J=1$ state does not lie between the two observed $J=3$ states. Furthermore the magnitude of the observed splittings is too large to be accounted for by the spin-orbit interaction of the Rydberg electron.

Another perturbation that seems to be of particular importance to the states under consideration is the electric-quadrupole interaction. The $6p_{3/2}nd$ configuration is mixed with the $6p_{1/2}\epsilon l$ continua via the quadrupole term in the two-electron electrostatic interaction. It has recently been demonstrated that the $6p_{3/2}nd$ and $6p_{3/2}ns$ states which lie above the $6p_{1/2}$ limit of Ba^+ are very strongly coupled to the $6p_{1/2}\epsilon l$ continua.[6,7] Similarly configuration interaction between $6p_{3/2}nl$ states with the $6p_{1/2}nl$ states implies a quadrupole interaction.[8] Presumably both

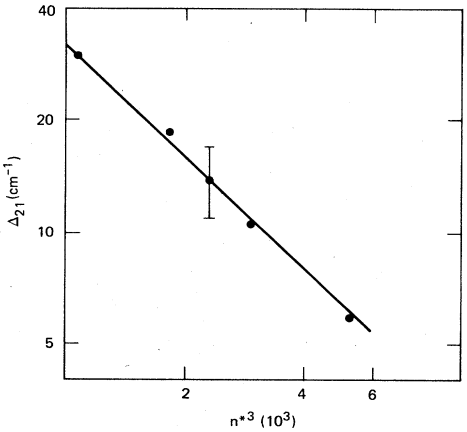

FIG. 3. Plot of Δ_{21} the energy separation between features I and II (see Fig. 2), plotted vs $(n^*)^3$ on a log-log plot. The solid line has a slope of -1.

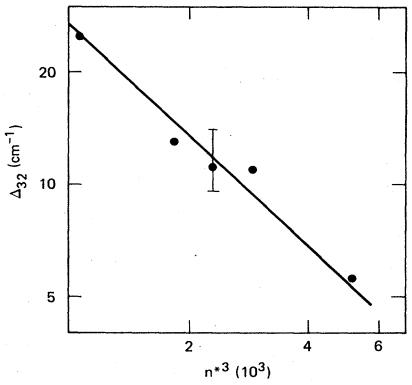

FIG. 4. Plot of Δ_{32} the energy separation between features III and II, plotted vs $(n^*)^3$ on a log-log plot. The solid line has a slope of -1.

these effects are due to the leading electric coupling, the electric quadrupole interaction. The quadrupole interaction will also lead to the splitting of the various J levels of the nominal $6p_{3/2}nd$ configuration. Finally in order to calculate the splittings correctly one must also take into account the exchange part of the electrostatic interaction and interactions of the type $\mathbf{S}_2\cdot\mathbf{L}_1$, where "2" refers to the Rydberg electron and "1" to the core electron. We have not attempted to pursue these calculations at present since the $6p_{3/2}nd_j$ states of Ba are fairly complex, involving a considerable amount of configuration mixing and a large number of open channels.

An intriguing aspect of our measurements is that no splittings between various J states were observed for the $(6p_{1/2}nd_j)_{J=1,3}$ series. In fact no differences were observed in the excitation spectra with linearly and circularly polarized lasers. (The quantum defects and the widths of the $J=3$ $6p_{1/2}nd_j$ states were measured by Gounand *et al.*[6]) Evidently the splittings of the J states belonging to the $(6p_{1/2}nd_j)_{J=1,3}$ series are smaller than the ~ 1 cm^{-1} resolution of our experiment, whereas the corresponding splittings for the $6p_{3/2}nd_j$ states are quite large. This is not surprising in light of the fact that the $6p_{1/2}nd_j$ states can have no direct quadrupole couplings with other $6p_{1/2}nl$ states and cannot be coupled via the electrostatic quadrupole interaction to the $6p_{3/2}\epsilon l$ continuum because they lie below the Ba^+ $6p_{3/2}$ limit.

V. MIXING OF THE $6p_{3/2}ns$ AND $6p_{1/2}nd$ STATES

The $6pnd$ $J=1$ or $J=3$ states are odd-parity states of $J=1$ and 3 which are only nominally of the configuration $6pnd$. By virtue of the fact that these states autoionize we know that they are coupled to the $6s\epsilon l$ and $5d\epsilon l$ continua. An interesting question is the extent to which they are coupled to, and therefore mixed with, other $6pnl$ states. The $6pnd$ $J=1$ states may be mixed with the $6pns$ states, and the $6pnd$ $J=3$ states may be mixed with the $6png$ states. To observe and measure such mixings, we have recorded the excitation spectra with high laser power which enhances the weak spectral features from such admixtures. Why this is a useful technique becomes apparent if the description of our excitation process is expressed using quantum-defect theory. Thus in this section we first review the basic notions of the quantum-defect theory description of the excitation process we use. We then present our experimental results and outline the quantum-defect theory used to generate synthetic spectra to extract the mixing of the $6p_{3/2}ns_{1/2}$ and $6p_{3/2}nd_j$ states.

Let us begin by considering the quantum-defect treatment of the excitation of a single series of autoionizing states when there is no state mixing. As this is treated in detail by Tran *et al.*,[2] Cooke and Cromer,[9] and Bhatti and Cooke,[10] here we merely summarize the salient features of the arguments. Consider the excitation of the prominent Ba $(6p_{3/2}nd_j)_{J=3}$ series from a bound $6snd$ state. We recall that this excitation process is essentially the Ba^+ $6s$-$6p$ transition with the outer electron remaining a spectator. This picture can be made quantitative using quantum-defect theory to write the photoexcitation cross section σ as

$$\sigma=\mu^2O^2(n_b,\nu)Z_d^2(\nu)\ , \tag{1}$$

where μ is the dipole matrix element of the Ba^+ $6s$-$6p$ transition, O is the overlap integral from the bound Rydberg $6snd$ state of effective quantum number n_b to an autoionizing $6pnd$ state of effective quantum number ν, and Z_d^2 is the density of the autoionizing Rydberg channel $6pnd$ which is periodic and peaks at the energies of the autoionizing $6pnd$ states. Note that ν is a continuous variable. For convenience it is useful to define ν_d, the effective quantum number of the $6pnd$ state, as the value of ν at the center of the $6pnd$ state. As μ is a constant the energy dependence of the cross section given in Eq. (1) arises from the variations of O and Z_d. If we follow the normal convention[10] of using Coulomb wave functions normalized per unit energy then $O^2=n_b^3$ when $\nu=n_b$ and $O=0$ for $\nu=n_b\pm i$, where i is an integer. In Fig. 5, we show plots of O^2 and Z_d^2 for the excitation of the $(6p_{3/2}nd_j)_{J=3}$ ($\nu_d\simeq 2.75$; the $J=3$, feature II listed in Table II gives $\nu_d=2.74$) series from the $6s\,15d\ ^1D_2$ state, for which $n_b=12.35$.

From Fig. 5 it is clear that the maximum value of the cross section occurs at the peak of Z_d^2 for which ν is nearest to n_b. Usually this occurs for $\nu\approx n_b$, where $O^2=n_b^3$ so that the cross section simply reflects Z_d^2 the profile of the autoionizing state. Under high-power excitation we are also able to observe the wings of the excitation cross section, corresponding to $|\nu-n_b|>1$, where the cross section is as much as three orders of magnitude smaller than it is at its peak value. From Fig. 5 it is evident that in the wings of the cross section the variations in both Z_d^2 and O^2 are important, as both oscillate with the same period. If, as is often the case, $\nu_d\approx n_b$ then the maxima in Z_d^2 are only slightly displaced from the zeros in O with the resulting asymmetric features shown in Fig. 5. Note that in Fig. 5 the subsidiary maxima of O occur at $\nu=n_b\pm i+\frac{1}{2}$, midway between successive values of ν_d, thus any $6pnd$ character, as reflected in Z_d^2, which has an effective quantum number $n_b\pm i+\frac{1}{2}$ is strongly enhanced in the observed spectra. In fact this is apparent in Fig. 5. Figure 5(a) shows that at $\nu=13.85$ the value of Z_d^2 is only 3% of its value at $\nu=14.35$, and yet, as shown by Fig.

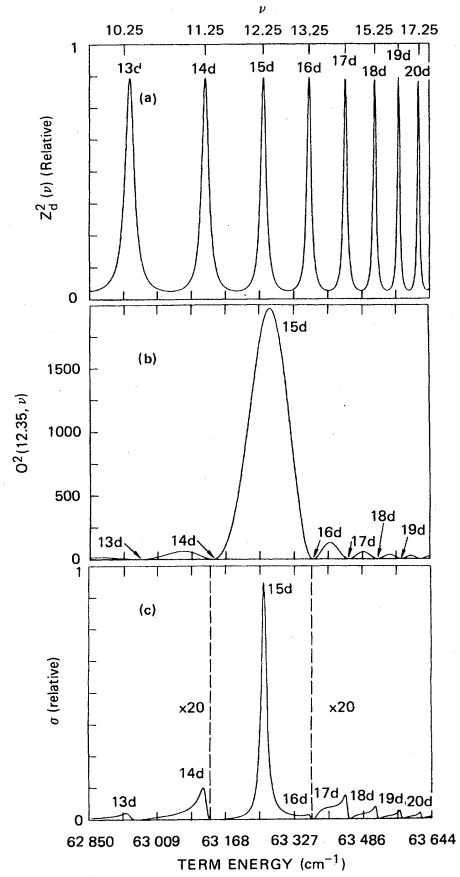

FIG. 5. (a) Plot of the density Z_d^2 of the $(6p_{3/2}nd_j)_{J=3}$ series near $6p_{3/2}15d_j$. Z_d^2 is a periodic function of ν, the width of the peaks being 10% of their spacing. (b) Plot of $O^2(12.35, \nu)$ the overlap integral squared from the $6s\,15d$ state $n_b=12.35$. Note the zeros at $\nu=12.35\pm i$, where i is an integer. (c) The calculated relative photoexcitation cross section from the bound $6s15d$ state.

5(c), the cross section is only a factor of 2 lower due to the variation in the overlap integral.

Now consider the effect of a small amount of configuration mixing, or channel mixing of the $6pnd$ and $6png$ $J=3$ states. This would result in the d states acquiring a small amount of g character and vice versa. Thus we would expect to find a small amount of d character in the $6png$ states. Stated another way, we would expect that Z_d^2 would show a small subsidiary peak at the locations of the $6png$ states. As the $6png$ states have a quantum defect of ~ 0.05 (Ref. 11) this subsidiary peak of Z_d^2 would be near the local maxima of the overlap integral at $\nu=12.35\pm i$ and would thus be strongly enhanced relative to the main peaks of Z_d^2 with $\nu=12.25\pm i$ which occur near the zeros of the overlap integral at $\nu=12.35\pm i$. Thus even quite small admixtures of d character in the g states should be quite apparent. The same reasoning implies that small admixtures of the $6pnd$ $J=1$ states into the $6pns$ $J=1$ states with quantum defects of 3.25 should also be easily observed. We are of course using the fact that the initial $6snd\ ^1D_2$ state has no $6sns$ or $6sng$ character.

Using high-power excitation, we have looked for the possible mixings of $6pnd$ states with other $6pnl$ states of the same odd parity and angular momentum. We are able to see quite clearly evidence of mixing of the $(6p_{3/2}nd_j)_{J=1}$ and $(6p_{3/2}ns_{1/2})_{J=1}$ states. However, for the $6p_{1/2}nd_j$ states, we observe no evidence of mixing with either the $6p_{1/2}ns_j$ or $6p_{1/2}ng_j$ states, nor do we observe any mixing of the $(6p_{3/2}nd_j)_{J=3}$ states with the $6p_{3/2}ng_j$ states.

In Figs. 6(a) and 7(a) we show high power spectra obtained with circular polarization of all three lasers from the Ba $6s\,15d\ ^1D_2$ and $6s\,17d\ ^1D_2$ states to the

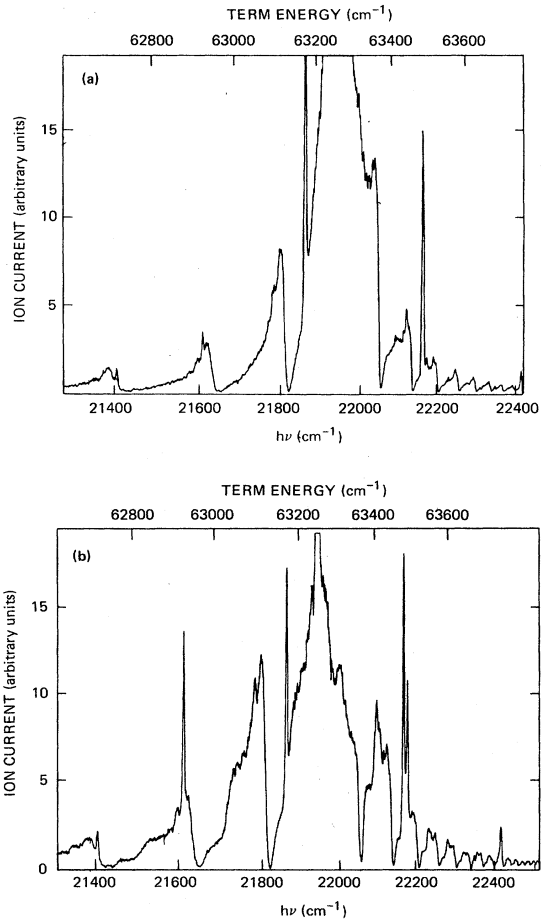

FIG. 6. High third laser power $6p_{3/2}nd_j$ spectra obtained with the $6s15d\ ^1D_2$ intermediate state. The sharp and narrow features seen in these experimental scans are the two-photon coincidence lines listed in Table I. (a) With all three lasers circularly polarized in the same sense to ensure the population of only $J=3$ autoionizing states. The spectrum is clearly reminiscent of Fig. 5(c). (b) With all three lasers collinearly polarized to allow the population of both $J=1$ and $J=3$ autoionizing states. Note the extra $J=1$ peaks which appear midway between the zeros in this spectrum. These peaks arise from the $(6p_{3/2}nd_j)_{J=1}$-$(6p_{3/2}ns_{1/2})_{J=1}$ mixing.

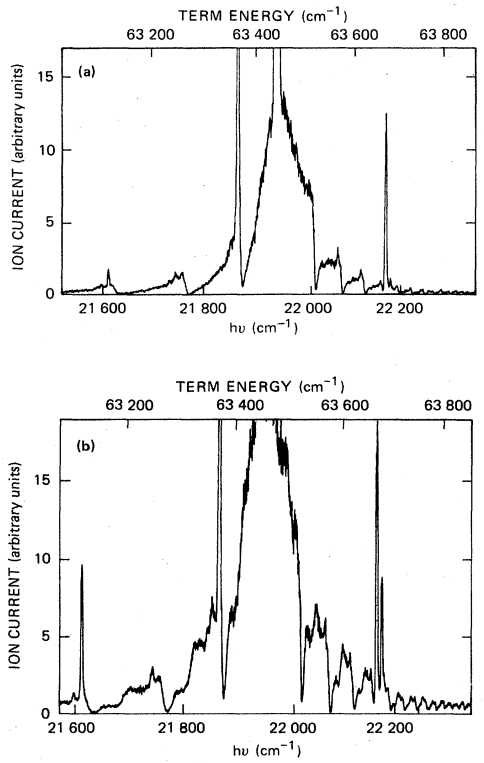

FIG. 7. High third laser power $6p_{3/2}nd_j$ spectra obtained with the $6s17d\ ^1D_2$ intermediate state. (a) With all three lasers circularly polarized in the same sense to ensure the population of only $J=3$ autoionizing states. The spectrum is clearly reminiscent of Fig. 5(c). (b) With all three lasers collinearly polarized to allow the population of both $J=1$ and $J=3$ autoionizing states. Note the extra $J=1$ peaks which appear midway between the zeros in this spectrum. These peaks arise from the $(6p_{3/2}nd_j)_{J=1}$-$(6p_{3/2}ns_{1/2})_{J=1}$ mixing.

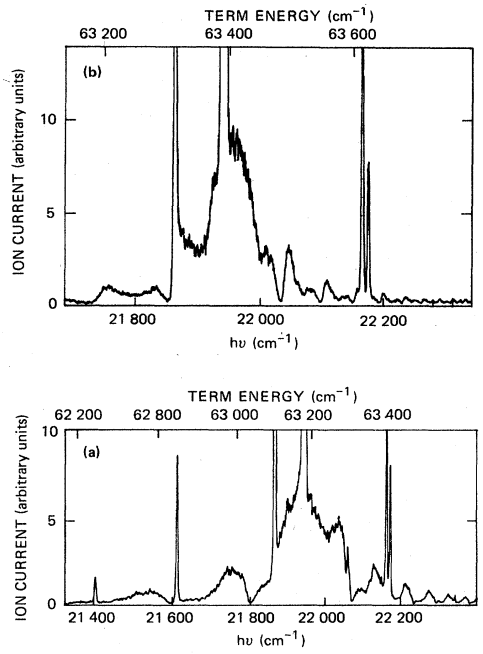

FIG. 8. High third laser power spectra of the $(6p_{3/2}ns_{1/2})_{J=1}$ states. (a) With the $6s16s\ ^1S_0$ state as intermediate state, (b) with the $6s18s\ ^1S_0$ state as intermediate state. As in Figs. 6(b) and 7(b) there is an extra peak in each of the subsidiary lobes which arises from the $(6p_{3/2}ns_{1/2})$-$(6p_{3/2}nd_j)$ mixing.

$(6p_{3/2}nd_j)_{J=3}$ channels, respectively. As noted in previous sections, although there are two $(6p_{3/2}nd_1)_{J=3}$ channels the excitation of the series with quantum defects 2.88 is negligible, and the observed spectra are thus the spectra of an unperturbed series of autoionizing states of quantum defect $\delta=2.75$ and width $0.1\nu^{-3}$ as shown in Fig. 5(c). As the $(6p_{3/2}ng_j)_{J=3}$ states have quantum defects of ~ 0.05,[11] any admixture of the $6p_{3/2}nd_j$ character into the $6p_{3/2}ng_j$ states would produce a feature at $\nu+i=0.95$, which we do not observe, as shown by Figs. 6(a) and 7. With linear, parallel polarization of all three lasers, which allows the population of $J=1$ and $J=3$ states, we see the spectra of Figs. 6(b) and 7(b) which exhibit additional features halfway between the zeros of Figs. 6 and 7. These features, which are evidently $J=1$, are at the locations of the $(6p_{3/2}ns_{1/2})_{J=1}$ states indicating that the $6pnd$ character is admixed in the $(6p_{3/2}ns_{1/2})_{J=1}$ state.

If the $6pnd$ state is admixed in the $6pns$ state then the reverse should also be true. In fact we find this to be the case. In Fig. 8, we show the spectra obtained from the $6s16s\ ^1S_0$ and $6s18s\ ^1S_0$ states as intermediate state. Neither of these spectra can be explained as arising from a single series of unperturbed autoionizing states. As we shall see, the spectra of Figs. 6(b), 7(b), and 8 can be reasonably reproduced by the inclusion of mixing of the $6pns$ and $6pnd$ series.

To quantify the mixing of the $6pnd$ and $6pns$ $J=1$ channels we must carry out a quantum-defect theory analysis of the autoionizing Ba $(6p_{3/2}nd_j)_{J=1}$ and $(6p_{3/2}ns_j)_{J=1}$ states. In fact there are a total of thirteen $J=1$ odd-parity channels above the Ba^+ $6p_{1/2}$ limit, the closed $6p_{3/2}ns_{1/2}$, $6p_{3/2}nd_{3/2}$, and $6p_{3/2}nd_{5/2}$ channels and ten continua. It is clear that little insight may be gained from such a complex model so we have chosen to reduce this problem to its essence and have considered a model in which there are two closed channels, $6pnd$ and $6pns$, and two open continuum channels. Specifically we chose the $6p_{3/2}nd_j$ state with quantum defect 2.62 as most of the excitation is to this channel. We number the four channels of this $J=1$ problem as shown in Table III.

We assume that the $6pnd$ states autoionize only to con-

TABLE III. Channels for four-channel $J=1$ analysis.

Channel label No.	Identification
1	$6pnd$
2	$6pns$
3	continuum 1
4	continuum 2

TABLE IV. Quantum defect and coupling of channels.

δ_1	quantum defect of channel 1 (closed)
δ_2	quantum defect of channel 2 (closed)
R'_{12}	coupling between the closed channels
R'_{13}	coupling of channel 1 to channel 3
R'_{23}	coupling of channel 2 to channel 3
R'_{24}	coupling of channel 2 to channel 4

tinuum 1 and the 6*pns* states to both continua. Furthermore we assume that the 6*pnd* and 6*pns* channels interact directly with each other.

To do the quantum-defect analysis, i.e., to calculate Z_d^2 and Z_s^2, we have used the formulation of Cooke and Cromer[9] which is similar to that developed by Seaton.[12] This formulation uses a parametrization in terms of collision channel properties, which conveniently matches out excitation method. Specifically the quantum defect of a series of unperturbed autoionizing states enters explicitly as one parameter, and its coupling to other collision channels both open and closed enters by different parameters.

In Table IV we list the relevant quantum-defect parameters for this four-channel analysis. The quantum defects δ_1 and δ_2 are familiar, they imply the energies of the 6*pnd* and 6*pns* states. The R'_{13}, R'_{23}, and R'_{24} parameters determine the autoionization widths. In the case $R'_{12}=0$ the autoionization widths [full width at half maximum (FWHM)] of the 6*pnd* and 6*pns* states are given by Γ_1 and Γ_2 where[8]

$$\Gamma_i=\frac{2}{\pi\nu_i^3}\sum_j R_{ij}'^2 . \tag{2}$$

Thus we see that the R'_{ij} parameters resemble the V coupling matrix elements used by Fano in his configuration interaction description of autoionizing states.[13] Finally we note that the parameter R'_{12} is analogous to a coupling matrix element between two bound states.

To compute the cross sections corresponding to the high-power spectra of Figs. 6–8 we begin with the reasonable assumption that only 6*pnd* channels which are easily excited are involved. Thus we consider the 6*pnd* $J=1$ and $J=3$ states with quantum defects of 2.62 and 2.75. Next we reduce the number of free parameters in the quantum-defect model by using the available low-power data. In fact all the parameters in Table IV save R'_{12}, R'_{23}, and R'_{24} may be determined from the existing low-power data. In addition we know that the total autoionization rate of the 6*pns* states is $0.14\nu_1^{-3}$ (Ref. 14) which constrains the sum of the squares of R'_{23} and R'_{24} of Table IV according to Eq. (2). Finally we recall that the spectra taken from the 6*snd* $^1D_2$ states with linear polarization are superpositions of the $J=1$ and $J=3$ spectra. Assuming the transitions are from a pure LS $^1D_2$ state to pure *jj*-coupled states, we calculate that the $J=3$ oscillator strength should be 50% larger than that for $J=1$. Thus we add the two calculated $J=3$ and $J=1$ cross sections in the ratio of 3:2 to arrive at the total cross section.

In previous sections we referred to the saturation, or depletion broadening, which occurs with high laser powers

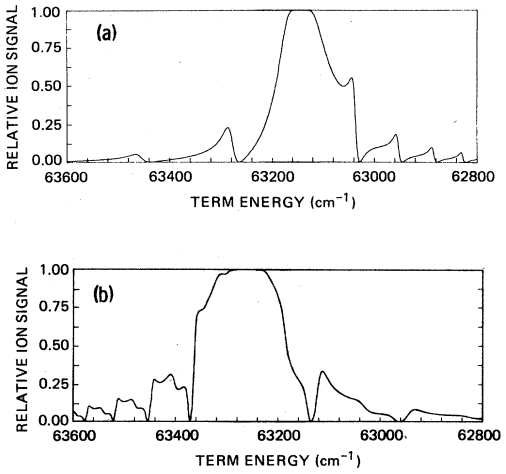

FIG. 9. Calculated spectra for the high third laser power excitation from the 6*s*15*d* $^1D_2$ state, (a) with all lasers circular polarized to populate only $J=3$ and assuming $N=140$, (b) with all lasers linear polarized to populate $J=1$ and 3 and assuming $N=200$.

and was first recognized by Cooke *et al.*[5] At the peak of the cross section, σ_m, the integrated photon flux ϕ of the third laser is so high that $\phi\sigma_m \gg 1$. Thus we observe signals comparable to those obtained at the peak of the cross section even for cross sections substantially smaller. The saturation, or depletion broadening can be taken into account by expressing the signal S as

$$S=1-e^{\frac{-\sigma N}{\sigma_m}} , \tag{3}$$

where $N=\phi\sigma_m$ is a measure of the saturation of the sig-

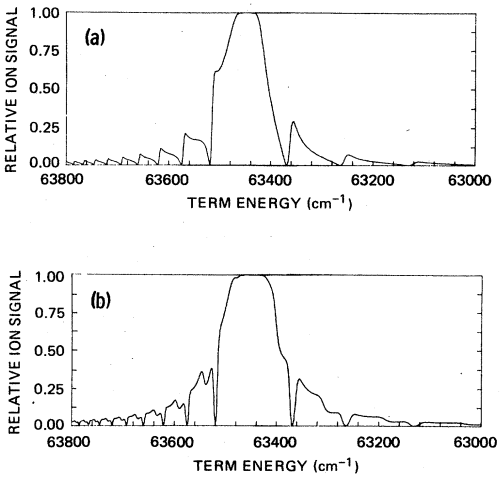

FIG. 10. Calculated spectra for the high third laser power excitation from the 6*s*17*d* $^1D_2$ state, (a) with all lasers circular polarized to populate only $J=3$ and assuming $N=140$, (b) with all lasers linear polarized to populate $J=1$ and 3 assuming $N=250$.

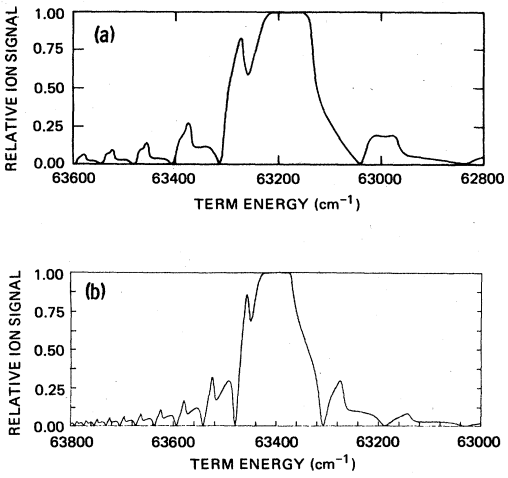

FIG. 11. Calculated spectra for the high third laser power excitation spectra from the (a) $6s16s\ ^1S_0$ state $N=200$ and (b) $6s18s\ ^1S_0$ state $N=170$.

nal at the maximum of the cross section.

To summarize, using quantum-defect theory we calculate the functions Z_d^2 and Z_s^2. These together with the appropriate overlap give the cross section as shown by Eq. (1). The $J=1$ and $J=3$ cross sections are added if necessary, and the depletion broadened spectrum is calculated using Eq. (3).

In Figs. 9—11, we show the calculated spectra. In Figs. 9(a) and 10(a) we show the calculated $J=3$ spectra from the $6s\,15d$ and $6s\,17d$ states. As noted earlier, for these spectra we have assumed that only the strongly excited $6p_{3/2}nd_j$ channel contributes, and since it is not coupled to the $6p_{3/2}ng$ channel this is effectively a two-channel problem. For consistency in notation, though, we treat the $J=3$ states with the four-channel model used previously for the $J=1$ states with the channels denoted as shown in Table V. If we set $R'_{12}=0$, our four-channel model reduces to two channels. The values of δ_1 and R'_{13} used in Figs. 9(a) and 10(a) are given in Table VI. It is clear that the spectra of Figs. 9(a) and 10(a) are reasonable facsimilies of those in Figs. 6(a) and 7(a).

In Fig. 9, we show the spectra calculated for linear polarization using the quantum-defect parameters listed in Table V. In our opinion, the reproduction of the experimental spectra is quite satisfactory. Using the same quantum-defect parameters of Table VI, but different saturation parameters, we calculate the spectra from the $6s16s$ and $6s18s$ states as shown in Fig. 11. In this case,

TABLE V. Channels for the $J=3$ analysis.

Channel label No.	Identification
1	$6pnd$
2	$6png$
3	continuum 1
4	continuum 2

TABLE VI. Multichannel-quantum-defect theory parameters.

	$J=1$	$J=3$
δ_1	0.62	0.75
δ_2	0.29	
R_{12}	0.20	0
R_{13}	0.50	0.47
R_{23}	0.30	
R_{24}	0.45	

the calculated spectra of Fig. 11 and observed spectra of Fig. 8 are in qualitative agreement. When we recall that all the s and d spectra are fit by the same parameters using the simplest possible model, we feel the agreement is quite good.

Using the quantum-defect parameters of Table VI we are able to calculate the values of Z_d^2 and Z_s^2 to show directly the admixture of $6pns$ into $6pnd$ and vice versa. In Fig. 12 we show plots of Z_s^2 and Z_d^2 over a small energy range encompassing one cycle of ν. As shown by Fig. 12 there is a small peak in the d character, Z_d^2, at the location of the $6p_{3/2}ns_j$ state and vice versa. Taking the ratios of the shaded areas in Fig. 11 to the areas under the main A_s^2 and Z_d^2 peaks indicates that there is a 5(2)% of d character mixed into the s channel and vice versa.

There are several interesting observations which may be made regarding this work. First, we note that it is clear that this is a problem in which more than one continuum is important, for our attempts to fit the data with a three-channel (one continuum) model failed by having a zero in Z_d at the maxima of Z_s and vice versa. Second, we note that the mixing of $6pns$ and $6pnd$ occurs mostly directly as reflected by R'_{12}. This is probably a direct quadrupole coupling which does not exist between the $6p_{1/2}ns_{1/2}$ and $6p_{1/2}nd_{3/2}$ states. This is supported by the observation of an analogous coupling between the

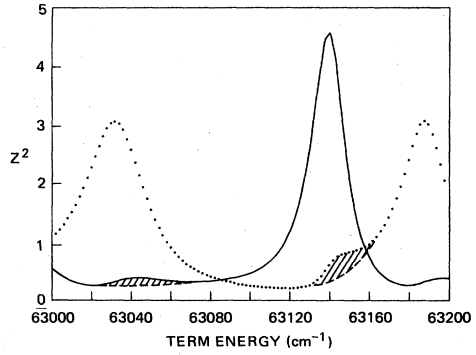

FIG. 12. Calculated values of Z_s^2(· · · ·) and Z_d^2(——) corresponding to Figs. 8(b), 9(b), and 10 over slightly more than one cycle of ν. The subsidiary peaks in Z_s^2 and Z_d^2 at the location of the primary peaks in Z_d^2 and Z_s^2 are quite evident. We have shown by the broken line (— — —) approximately what Z_d^2 and Z_s^2 would be without the mixing. The shaded area (///) is thus the amount of mixing.

$6p_{3/2}ns_j$ and $6p_{1/2}nd_j$ states by Bhatti *et al.*[8] and the electron spectroscopy results of Kachru *et al.*[7] The indirect coupling, through the continuum channel 3 leads to shifts in the energy of admixtures. We found that for $R'_{23}>0$ the *nd* satellite at the energy of the *ns* state moved to higher energy and for $R'_{23}<0$ it moved to lower energy. Our experiments indicated that the former is the case.

VI. CONCLUSION

The results of this work indicate that there are observable ΔJ splittings of the autoionizing Ba $6p_{3/2}nd_j$ states but not of the $6p_{1/2}nd_j$ states. Furthermore we are able to observe the very small, 5%, mixing of the $(6p_{3/2}nd_j)_{J=1}$ and $(6p_{3/2}ns_{1/2})_{J=1}$ series, using a novel technique that amplifies the effects of such mixings. However, a similar mixing is not observed in $(6p_{1/2}nd_j)_{J=1}$ and $(6p_{1/2}ns_{1/2})_{J=1}$ states. Nor is it observed between the $(6p_jnd_j)_{J=3}$ and $(6p_jng_j)_{J=3}$ states. All these observations are consistent with an electric quadrupole interaction which is forbidden for the $6p_{1/2}nl_j$ states and is expected to fall off rapidly with increasing l of the outer electron.

ACKNOWLEDGMENTS

It is a pleasure to acknowledge helpful discussions with W. E. Cooke and D. L. Huestis on various aspects of these problems. This work was supported by National Science Foundation Grant No. PHY-83-06082.

[1]W. E. Cooke and T. F. Gallagher, Phys. Rev. Lett. **41**, 1648 (1978).
[2]N. H. Tran, P. Pillet, R. Kachru, and T. F. Gallagher, Phys. Rev. A **29**, 2640 (1984).
[3]J. R. Rubbmark, S. A. Borgstrom, and K. Bockastem, J. Phys. B **10**, 421 (1977).
[4]W. E. Cooke, T. F. Gallagher, S. A. Edelstein, and R. M. Hill, Phys. Rev. Lett. **43**, 1239 (1979).
[5]W. E. Cooke, S. A. Bhatti, and C. L. Cromer, Opt. Lett. **7**, 69 (1982).
[6]F. Gounand, T. F. Gallagher, W. Sandner, K. A. Safinya, and R. Kachru, Phys. Rev. A **27**, 1925 (1983).
[7]W. Sandner, R. Kachru, K. A. Safinya, F. Gounand, W. E. Cooke, and T. F. Gallagher, Phys. Rev. A **27**, 1717 (1983); R. Kachru, N. H. Tran, P. Pillet, and T. F. Gallagher, Phys. Rev. A **31**, 218 (1985).
[8]S. A. Bhatti, C. L. Cromer, and W. E. Cooke, Phys. Rev. A **24**, 161 (1981).
[9]W. E. Cooke and C. L. Cromer (unpublished).
[10]S. A. Bhatti and W. E. Cooke, Phys. Rev. A **28**, 756 (1983).
[11]S. M. Jaffe (private communication).
[12]M. J. Seaton, Rep. Prog. Phys. **46**, 167 (1983).
[13]U. Fano, Phys. Rev. **124**, 1866 (1961).
[14]W. E. Cooke (private communication).